Oxymetholone Therapy of Fanconi Anemia Suppresses Osteopontin Transcription and Induces Hematopoietic Stem Cell Cycling

Qing-Shuo Zhang,[1,*] Eric Benedetti,[1] Matthew Deater,[1] Kathryn Schubert,[1] Angela Major,[2] Carl Pelz,[1] Soren Impey,[1] Laura Marquez-Loza,[1] R. Keaney Rathbun,[3] Shigeaki Kato,[4] Grover C. Bagby,[3] and Markus Grompe[1]

[1]Oregon Stem Cell Center, Department of Pediatrics, Oregon Health & Science University, Portland, OR 97239, USA
[2]Department of Pathology, Texas Children's Hospital, Houston, TX 77030, USA
[3]NW VA Cancer Research Center, VA Medical Center Portland, Portland, OR 97239, USA
[4]Institute of Molecular and Cellular Biosciences, The University of Tokyo, Tokyo 113-0032, Japan
*Correspondence: zhangqi@ohsu.edu
http://dx.doi.org/10.1016/j.stemcr.2014.10.014

SUMMARY

Androgens are widely used for treating Fanconi anemia (FA) and other human bone marrow failure syndromes, but their mode of action remains incompletely understood. Aged $Fancd2^{-/-}$ mice were used to assess the therapeutic efficacy of oxymetholone (OXM) and its mechanism of action. Eighteen-month-old $Fancd2^{-/-}$ mice recapitulated key human FA phenotypes, including reduced bone marrow cellularity, red cell macrocytosis, and peripheral pancytopenia. As in humans, chronic OXM treatment significantly improved these hematological parameters and stimulated the proliferation of hematopoietic stem and progenitor cells. RNA-Seq analysis implicated downregulation of osteopontin as an important potential mechanism for the drug's action. Consistent with the increased stem cell proliferation, competitive repopulation assays demonstrated that chronic OXM therapy eventually resulted in stem cell exhaustion. These results expand our knowledge of the regulation of hematopoietic stem cell proliferation and have direct clinical implications for the treatment of bone marrow failure.

INTRODUCTION

Fanconi anemia (FA) is an autosomal recessive disorder associated with birth defects, progressive bone marrow failure, hematopoietic stem cell (HSC) depletion, and cancer predisposition. FA is caused by a disrupted FA-BRCA network and is genetically heterogeneous, with at least 16 complementation groups and respective genes identified so far (Kim and D'Andrea, 2012).

Progressive bone marrow failure is the primary cause of morbidity and mortality in FA patients (Kutler et al., 2003). Most patients develop marrow dysfunction within the first decade of life. The symptoms range from mild cytopenia in any lineage to severe aplastic anemia, often initially with thrombocytopenia (Shimamura and Alter, 2010). Red cell macrocytosis is quite common in FA patients and usually precedes the onset of thrombocytopenia.

HSC transplantation is the only curative treatment for bone marrow failure in FA. However, androgens have also been widely used to treat cytopenia in FA, especially for patients unable to proceed to transplant or patients with high transplant risk. The most commonly used androgen is oxymetholone (OXM), which is an anabolic-androgenic steroid and a synthetic derivative of testosterone (Shimamura and Alter, 2010). Androgen therapy raises blood counts in ~50% to 70% of individuals with FA and also works for other forms of aplastic anemia (Dokal, 2003).

Despite a long history of androgen use in bone marrow failure syndromes, the mechanism whereby these molecules boost blood counts remains enigmatic (Chute et al., 2010). It has been suggested that androgens stimulate erythropoiesis through an increase in the production of erythropoietin (EPO). However, more recent studies have found no close correlation between androgens and EPO levels (Chute et al., 2010), leading others to speculate that androgens might have a direct effect on bone marrow (T'Sjoen et al., 2005). One recent in vitro study suggested that androgens act by increasing telomerase activity and extending the lifespan of CD34+ stem/progenitor cells (Calado et al., 2009).

Multiple murine models of FA are available. Among them, $Fancd2^{-/-}$ mice, $Fancp^{-/-}$ mice, and $Fancc$-$Fancg$ double knockout mice represent human FA patient phenotypes more closely than the others (Crossan et al., 2011; Houghtaling et al., 2003; Parmar et al., 2010; Pulliam-Leath et al., 2010; Zhang et al., 2010). $Fancd2^{-/-}$ mice recapitulate the characteristic tumor susceptibility of FA and show an ~2-fold decrease in hematopoietic stem and progenitor cell (HSPC) populations and a very poor long-term repopulating capacity of bone marrow (Parmar et al., 2010; Zhang et al., 2010). Despite this, the mice have no obvious anemia in their peripheral blood at age 6 months, except for lower platelet counts. Here, however, we found that 18-month-old $Fancd2^{-/-}$ mice developed spontaneous pancytopenia. We then set out to investigate how OXM benefits FA patients using this aged $Fancd2^{-/-}$ mouse model.
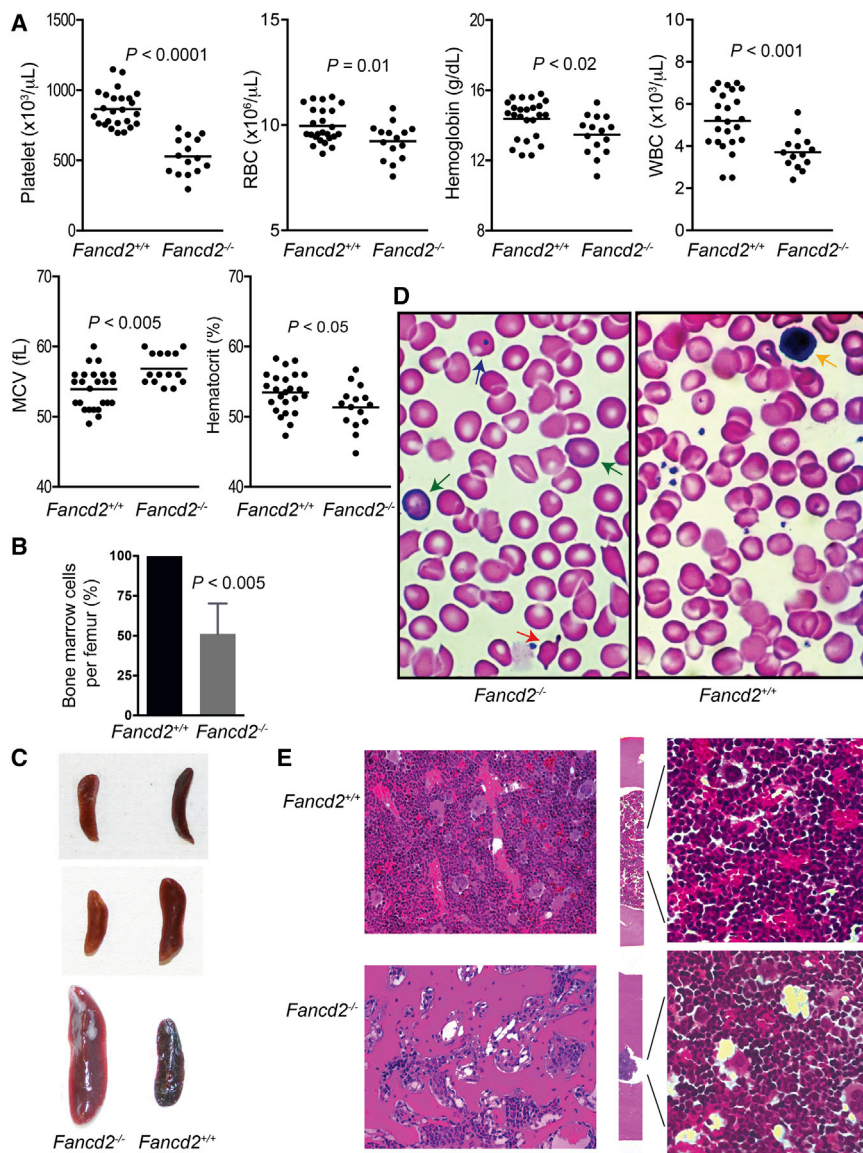
CrossMark

Figure 1. Eighteen-Month-Old *Fancd2*$^{-/-}$ Mice Have Pancytopenia

(A) Complete blood counts in 18-month-old *Fancd2*$^{-/-}$ mutants (n = 15) and WT controls (n = 25). WBC, white blood cells; RBC, red blood cells.

(B) Reduced bone marrow cellularity in *Fancd2*$^{-/-}$ mice. Total nucleated bone marrow cells were counted for each femur bone. The data showed the relative change (as percentage) of marrow cellularity in mutant mice as compared with their littermate WT controls and represented pooled results from four pairs of mice.

(C) *Fancd2*$^{-/-}$ mice have spleen abnormalities. (Upper and middle panels) Small spleens in two mutant mice. (Lower panel) Larger spleen in a mutant mouse.

(D) Representative blood smear pictures of *Fancd2*$^{-/-}$ mice and gender-matched WT littermate controls. The blue arrow indicates a Howell-Jolly body; green arrow, polychromatic cells; orange arrow, acanthocyte; yellow arrow, lymphocyte. Original magnification ×1,000.

(E) H&E staining of the bone sections. (Left) Longitudinal section of the trabecular bones (original magnification, ×100). (Middle and right) Longitudinal section of the cortical bones (original magnifications: middle panels, × 50; right panels, × 400). See also Table S1.

RESULTS

Eighteen-Month-Old Fancd2$^{-/-}$ Mice Have Pancytopenia and Respond to OXM Treatment

We previously reported that 4- to 6-month-old *Fancd2*$^{-/-}$ mice have reduced numbers of HSCs with no evidence for anemia in peripheral blood except for low platelet counts (Zhang et al., 2010, 2013). A follow-up investigation on a larger cohort of mice at the same age confirmed normal white and red blood cell counts and low platelet counts and also revealed a slight but significant elevation of mean corpuscular volume (MCV), which is a characteristic clinical phenotype of human FA patients (Table S1 available online) (Shimamura and Alter, 2010). To track

the progression of these defects, we followed a cohort of *Fancd2*$^{-/-}$ and WT mice until 18 months of age. Similar to the findings in our earlier report (Houghtaling et al., 2003), 5 of 17 mutant mice developed tumors (with 3 of them being ovarian tumors) during this time period, whereas only 1 of 20 WT mice had a tumor. Animals with tumors were excluded from further analysis. We found that cancer-free 18-month-old *Fancd2*$^{-/-}$ mice had developed spontaneous pancytopenia with red blood cells, white blood cells, hemoglobin levels, and platelet counts all below the normal ranges seen in age-matched WT controls (Figure 1A). *Fancd2*$^{-/-}$ mice also showed a highly elevated MCV compared with WT controls and a reduction in bone marrow cellularity ranging from 25% to 75%
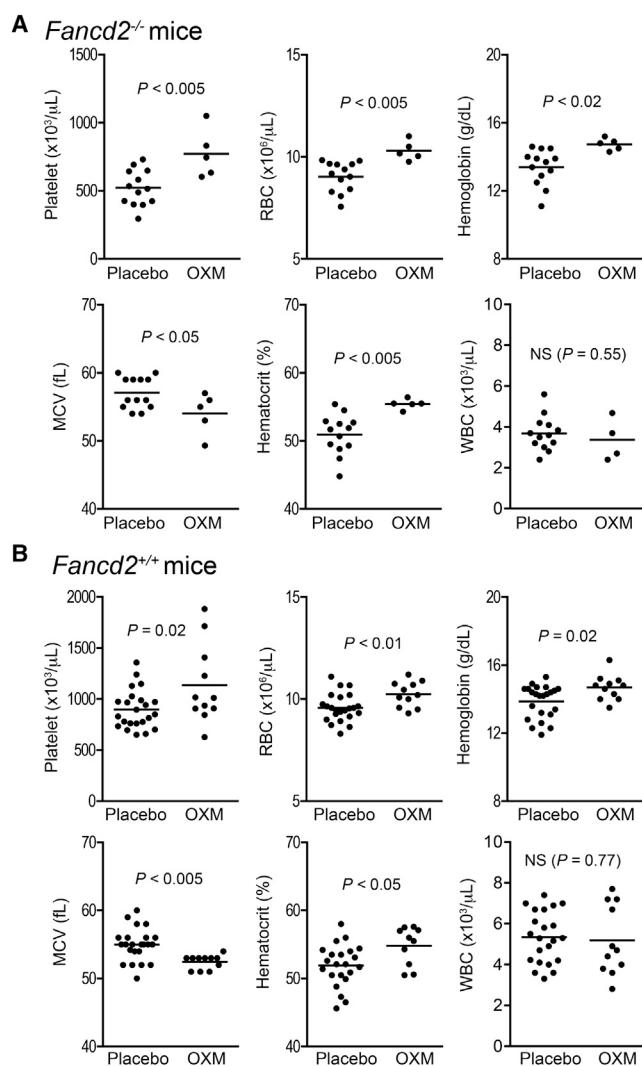
Figure 2. OXM Treatment Improves Hematopoiesis
(A) OXM-treated *Fancd2*$^{-/-}$ mice (n = 5) exhibited better hematologic parameters than placebo-treated *Fancd2*$^{-/-}$ controls (n = 13).
(B) OXM-treated *Fancd*$^{+/+}$ mice (n = 11) had better hematologic parameters than placebo-treated *Fancd2*$^{+/+}$ controls (n = 23). OXM treatment started at weaning and continued for 17 months before final harvest.
See also Figure S1.

(Figures 1A and 1B). Most of the old *Fancd2*$^{-/-}$ mice showed spleen defects, with 6 of 10 mice displaying small spleens and 2 of 10 mice having splenomegaly (Figure 1C). We consistently observed Howell-Jolly bodies, which are often associated with decreased splenic function, in peripheral blood smears (Figure 1D). Large, oval-shaped macrocytes and polychromatic cells (bluish red blood cells in hematoxylin and eosin [H&E] staining) were also visible in the peripheral blood of 18-month-old *Fancd2*$^{-/-}$ mice

(Figure 1D). In contrast, they were rare in age-matched WT mice. Four of 10 of the old *Fancd2*$^{-/-}$ mice had thickening of the cortical bone and narrowing of the marrow cavity typical of osteopetrosis (Figure 1E).

We next wished to test whether OXM could improve these FA-associated hematologic abnormalities. The OXM dose was chosen to be equivalent to ∼80% of the maximum dose for human patients (Shimamura and Alter, 2010). To assure that the compound had the expected biological activity, *Fancd2*$^{-/-}$ and WT mice were treated with either OXM-supplemented or placebo chow for 4 months. At harvest OXM-treated animals had larger kidneys (Figures S1A and S1B), indicating that the androgenic dose was sufficient and biologically active (Shukla et al., 1992). Androgen is known to downregulate renal ornithine aminotransferase gene *Oat* (Levillain et al., 2005). As expected, *Oat* mRNA expression level in OXM-treated mice was reduced by 75% (Figure S1C), further confirming the bioactivity of the OXM diet.

We then treated cohorts of 1-month-old *Fancd2*$^{-/-}$ mice and WT littermate controls with either OXM-supplemented chow or placebo diet and monitored them until age 18 months. Importantly, mice on OXM exhibited clearly improved hematological parameters, including platelet counts, red blood cell counts, hematocrit, and hemoglobin levels (Figures 2A and 2B), albeit with no significant changes in white blood cell counts. The long-term OXM treatment also partially corrected the macrocytosis typical for FA. Collectively, these results indicate that 18-month-old *Fancd2*$^{-/-}$ mice recapitulated FA patient phenotypes and that OXM benefited *Fancd2*$^{-/-}$ mice at the level of peripheral blood in the same way it does for human patients.

Long-Term OXM Treatment Leads to Stem Cell Exhaustion in Both Fancd2$^{-/-}$ and WT Mice

We then sought to determine the effect of long-term OXM administration on bone marrow HSPCs, immunophenotypically defined as c-KIT$^+$SCA-1$^+$LIN$^-$ (KSL) cells. Cohorts of 1-month-old *Fancd2*$^{-/-}$ and WT mice were treated with either OXM-supplemented chow or placebo diet and monitored until age 18 months. CD34$^-$KSL cells, a population enriched with long-term HSCs, were then quantitated by flow cytometry (Figure 3A). First, we compared the frequencies of CD34$^-$KSL cells in these old mice with those in young mice. As shown in Figure 3B, 18-month-old *Fancd2*$^{-/-}$ mice had significantly fewer CD34$^-$KSL cells than 4-month-old *Fancd2*$^{-/-}$ mice, indicating a progressive attrition of the HSC pool during the aging process. We then examined the effect of OXM on the frequencies of CD34$^-$KSL cells. Surprisingly, the CD34$^-$KSL proportions of the nucleated bone marrow cells in OXM-treated *Fancd2*$^{-/-}$ and WT mice (0.005% and 0.019%, respectively)

were significantly lower (p < 0.05 for WT and p < 0.02 for $Fancd2^{-/-}$ mice) than those in placebo-treated $Fancd2^{-/-}$ and WT mice (0.009% and 0.027%, respectively), as shown in Figure 3B. These results indicate that long-term OXM administration might cause stem cell exhaustion.

We next evaluated the function of the HSCs from these older mice with the competitive repopulation assay depicted in Figure 3C. Bone marrow cells of OXM-treated mice were transplanted along with a fixed ratio of $ROSA26^{Tg/O}$ genetically marked bone marrow cells (as competitors) into lethally irradiated $Fancc^{-/-}$ mice. Six months after transplantation, peripheral blood chimerism was measured using quantitative PCR for the three genotypes. At transplantation, the donor mix contained $Fancd2^{-/-}$ bone marrow cells and $ROSA26^{Tg/O}$ bone marrow cells at a 3:1 ($Fancd2^{-/-}$ versus $ROSA26^{Tg/O}$) ratio. Six months after transplantation, this ratio for placebo-treated $Fancd2^{-/-}$ bone marrow dropped to 1:150 (Figure 3D). This decrease in repopulating ability is significantly worse than that of 3-month-old $Fancd2^{-/-}$ mice under similar experimental settings previously reported by us (Zhang et al., 2010, 2013) and suggests a progressive deterioration of long-term HSC function in $Fancd2^{-/-}$ mice as they age. In contrast, placebo-treated WT bone marrow cells only suffered marginal loss in their HSC repopulating capacity with aging (Figure 3D). Interestingly and importantly, the long-term HSC repopulating capacities of both $Fancd2^{-/-}$ and WT bone marrow were reduced by ∼40% (p < 0.05) in OXM-treatment groups (Figure 3D). Taken together, these data indicate that OXM administration leads to loss of long-term HSC function.

OXM Selectively Stimulates HSPC Proliferation in Both Fancd2$^{-/-}$ and WT Mice

Increased cell cycle entry has been associated with eventual stem cell exhaustion in several models (Orford and Scadden, 2008). To understand what drove the loss of long-term HSC function after chronic OXM administration, the cell cycle status of HSPCs in OXM-treated mice was determined. $Fancd2^{-/-}$ mice and controls were given either OXM diet or placebo for 4 months starting at 1 month of age. We previously reported that $Fancd2^{-/-}$ KSL cells lose quiescence and display enhanced cell cycle entry (Zhang et al., 2010, 2013). Four months of OXM therapy were insufficient to change the size of HSPC pool or affect HSPC function in the colony-forming unit-spleen assay (data not shown). Nonetheless, cell cycle analysis at this time revealed that OXM administration profoundly stimulated the proliferation of HSPCs. The cell cycle status was measured with a well-established method combining Hoechst 33342 staining (for DNA content) with intracellular KI67 expression (expressed only in cycling cells, not in quiescent G0 cells). As shown in Figure 4A, both

$Fancd2^{-/-}$ and $Fancd2^{+/+}$ mice on OXM treatment had substantially fewer quiescent G0 KSL cells and a higher percentage of actively cycling ones (S-G2-M phases of the cell cycle) than their placebo-treated littermate controls. Upon OXM administration, the average G0 percentage of KSL cells in $Fancd2^{-/-}$ and $Fancd2^{+/+}$ mice dropped from 24.1% and 48.4% to 14.0% and 35.1%, respectively (p < 0.0001 for both) (Figure 4B). Correspondingly, the average S-G2-M proportions of KSL cells increased from 16.2% to 22.9% in mutant animals (p < 0.002) and from 9.4% to 13.0% in WT mice (p < 0.05) (Figure 4B). These results indicate that OXM further enhanced the already accelerated proliferation of FA HSPCs and drove them into active cycling.

We then determined whether the proliferation-enhancing effect of OXM was specific only to HSPCs. The cell cycle profiles of more mature lineage-positive (LIN$^+$) cells from the same mice were evaluated. We found that $Fancd2^{-/-}$ LIN$^+$ cells had a normal cell cycle status (Figure 4C). Interestingly, the G0 and S-G2-M proportions of LIN$^+$ cells were unchanged after OXM administration in both mutant and WT (Figures 4C and S2). In addition, we also examined the cell cycle status of LIN$^-$c-KIT$^+$SCA-1$^-$ cells, a population that includes common myeloid progenitors, granulocyte/monocyte progenitors, megakaryocyte/erythroid progenitors, and other cells. Although $Fancd2^{-/-}$ LIN$^-$c-KIT$^+$SCA-1$^-$ cells showed slightly reduced quiescence compared with their WT counterparts, neither $Fancd2^{-/-}$ nor WT LIN$^-$c-KIT$^+$SCA-1$^-$ cells showed increased proliferation in response to OXM administration (Figure S3). These results indicated that OXM did not broadly stimulate blood cell proliferation, but acted selectively at the level of HSPCs.

RNA-Seq Analysis Discovers Transcriptional Changes in Fancd2$^{-/-}$ HSPCs

We next wished to compare the transcriptomes of Fanconi mutant and normal HSPCs. KSL cells were sorted by flow cytometry after 3 months of OXM administration and used for RNA-Seq gene expression analysis (Wang et al., 2009). Three individual samples (pooled from five mice for each sample) were processed for each experimental condition, with combined reads (aligned to unique RefSeq genes) per condition in the range of 100 to 200 million. As shown in Table S2, $Fancd2^{-/-}$ KSL cells showed clear changes in mRNA expression profiles compared with WT controls: 430 genes were downregulated by more than 1.5-fold, whereas 159 genes were upregulated. As expected from previous work (Houghtaling et al., 2003), we observed a 2.5-fold reduction of $Fancd2$ mRNA expression level in $Fancd2^{-/-}$ KSL cells, confirming the reliability of the RNA-Seq analysis. Whole bone marrow cells were also analyzed in parallel; genes enriched in KSL cells as compared with
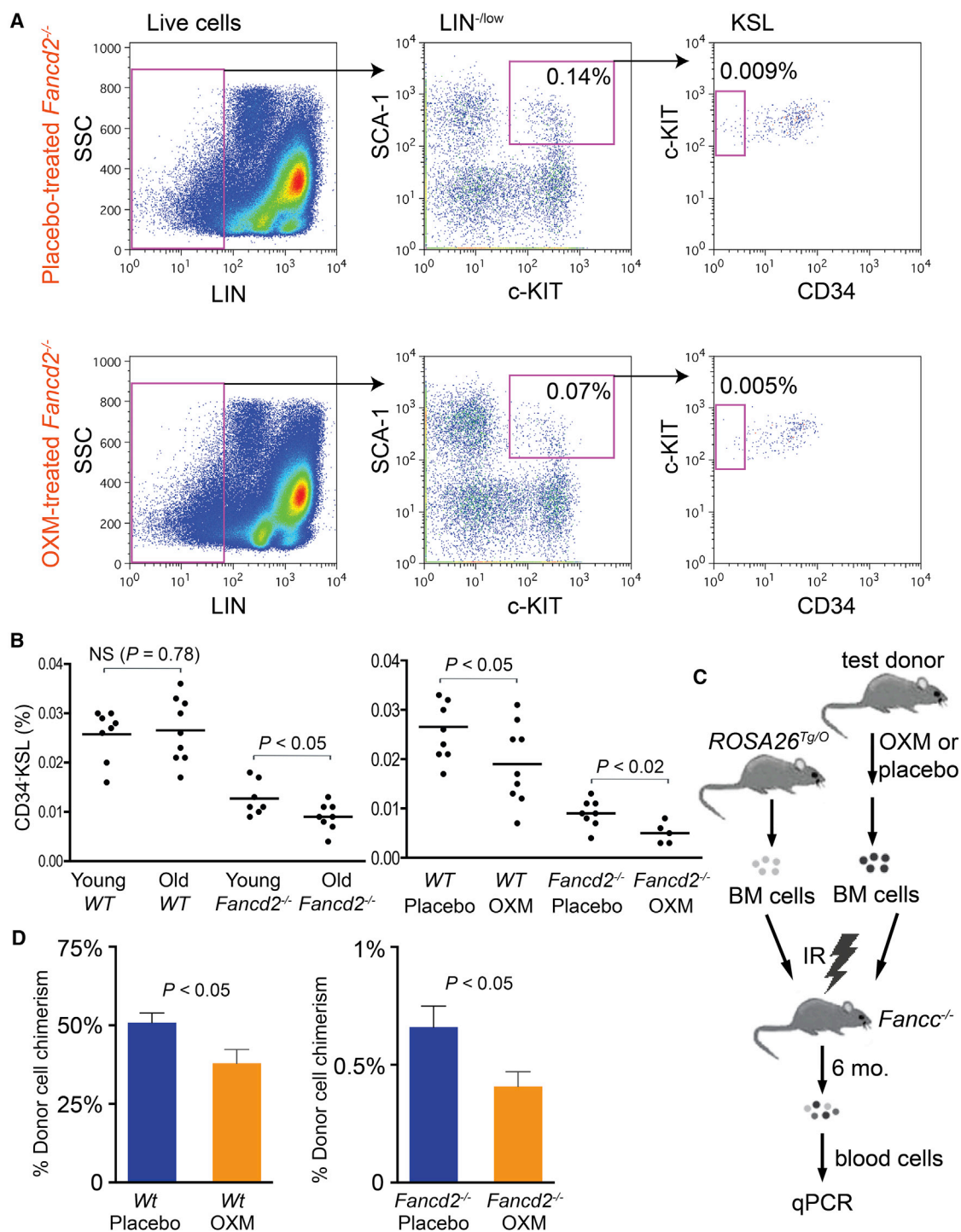
Figure 3. Long-Term OXM Treatment Leads to Stem Cell Exhaustion in Both *Fancd2*^{−/−} and WT Mice

(A) Long-term (18 months) OXM administration in *Fancd2*^{−/−} mice reduced the size of bone marrow CD34^{−}KSL cell population. Percentages on flow cytometry profiles were the mean of five to nine mice.

(B) Statistical quantification of CD34^{−}KSL cell proportion in whole nucleated bone marrow cells. (Left) Comparison of CD34^{−}KSL cell frequency between 4- to 6-month-old and 18-month-old mice. (Right) Comparison of CD34^{−}KSL cell frequency between 18-month-old mice on OXM treatment and those on placebo treatment. All the data are pooled results from multiple mice (n = 5–9 for each group).

(C) Strategy used in the competitive repopulation experiment. IR, BM, and mo denote irradiation, bone marrow and months, respectively.
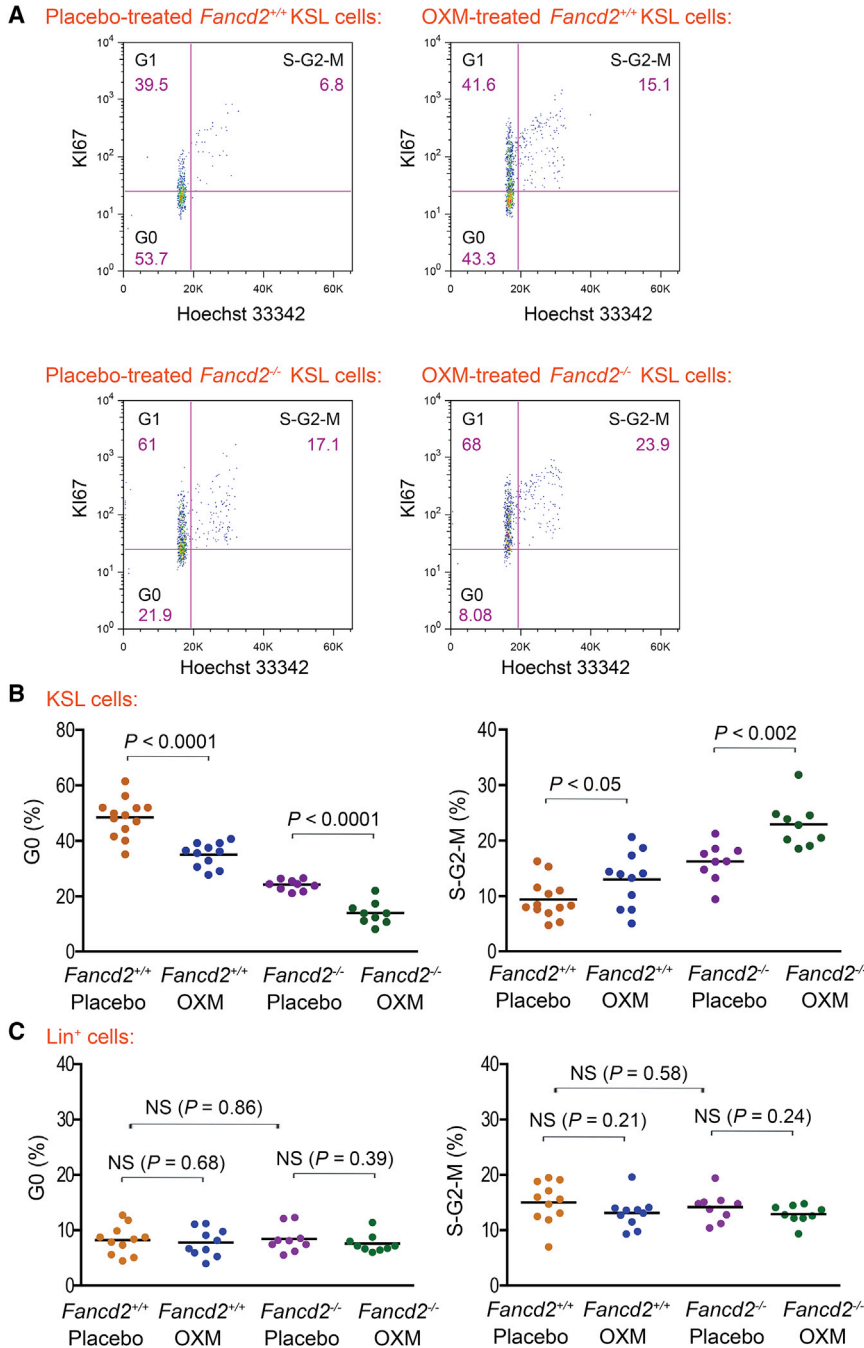
(legend continued on next page)

Figure 4. OXM Selectively Stimulates Proliferation of KSL Cells in Both *Fancd2*$^{-/-}$ and *Fancd2*$^{+/+}$ Mice

(A) Representative cell cycle profiles of KSL cells from OXM-treated mice and their gender-matched placebo-treated littermate controls. Hoechst 33342 (for DNA content) and FITC-conjugated antimouse KI67 (for G0/G1 discrimination) were used in combination to distinguish cells in G0, G1, and S-G2-M phases of the cell cycle. The denoted percentage for each gate was from a typical experiment. The mean percentage of multiple mice for each group was shown in the main text.

(B) Statistical quantification of the cell cycle analysis on KSL cells in OXM- versus placebo-treated mice. Data represent the mean values from multiple mice (n = 9 for both OXM and placebo groups of *Fancd2*$^{-/-}$ mice, n = 13 for *Fancd2*$^{+/+}$ placebo group, and n = 11 for *Fancd2*$^{+/+}$ OXM group).

(C) Statistical quantification of the cell cycle analysis on LIN$^+$ cells in OXM- versus placebo-treated mice. Data represent the mean values from multiple mice (n = 9 for either OXM or placebo group of *Fancd2*$^{-/-}$ mice, n = 11 for *Fancd2*$^{+/+}$ placebo group, and n = 10 for *Fancd2*$^{+/+}$ OXM group).

See also Figures S2 and S3.

whole bone marrow cells are listed in Table S3. The transcriptional downregulation (by 1.8-fold) of *Cdkn1c* in *Fancd2*$^{-/-}$ KSL cells is particularly interesting since its protein product p57 is critically required for maintaining quiescence in long-term HSCs (Tesio and Trumpp, 2011). Consistent with its important function in HSCs, our data

(D) In vivo competitive repopulation of OXM-treated (or control) test donor bone marrow and *ROSA26*$^{Tg/0}$ competitor bone marrow cells. Three donors were evaluated for each experimental group; % chimerism refers to the percentage of test donor-derived cells in all donor-derived cells. Results from multiple recipients (seven to nine mice per group) were pooled together for each experimental group. Data are presented as mean ± SEM.
See also Table S8.

Table 1. Pathways Significantly Changed in *Fancd2*⁻/⁻ HSPCs as Compared with WT HSPCs

Pathway	Change	FDR Score[a]
Cell differentiation	down	0.001
Cell cycle and its regulation	up	0.002
Mitogenic signaling	down	0.016
Nuclear receptor signaling	down	0.022
Inflammatory and immune response	up	0.060

[a]FDR denotes false discovery rate. The FDR cutoff for pathway analyses was set at 0.10. Detailed gene lists for some important pathways were shown in Table S4. See also Tables S2 and S3.

Table 2. Genes Differentially Changed in Both *Fancd2*⁻/⁻ and WT HSPCs in Response to OXM Administration

Gene	Symbol	Gene ID	Fold Change	Q Value[a]
Centromere protein F	*Cenpf*	NM_001081363	1.5	0.000
Marker of proliferation Ki-67	*Mki67*	NM_001081117	1.4	0.000
Secreted phosphoprotein 1	*Spp1*	NM_009263	−10.5	0.025
2′-5′ oligoadenylate synthetase-like 2	*Oasl2*	NM_011854	−1.5	0.03

[a]Q value cutoff was set at 0.05. See also Figure S6 and Tables S5 and S7.

showed that *Cdkn1c* transcript was enriched by 23-fold in KSL cells as compared with whole bone marrow cells (Table S3). In addition, the critical DNA-damage response gene Rad51 was also upregulated in *Fancd2*⁻/⁻ KSL cells as expected since FA cells often show persistent DNA damage foci due to insufficient DNA interstrand crosslink repair.

Gene ontology analysis revealed key pathways to be significantly altered in *Fancd2*⁻/⁻ KSL cells (summarized in Table 1). Consistent with the abnormal cell cycle status discovered by flow cytometry analysis, the pathways of cell cycle activation and its regulation were enhanced in *Fancd2*⁻/⁻ KSL cells. Specifically, many cell cycle genes showed transcriptional changes in *Fancd2*⁻/⁻ KSL cells, including the upregulation of *Cdk1*, *Ccna2*, *Ccnb1*, *Ccnb2*, *Ccnd1*, *Cdc25C*, *Cdkn3*, *Cdca3*, *Cdca8*, *Cks1b*, *Nek2*, *Birc5*, *Cdca5*, *Mad2l1*, *Pttg1*, and *Aurka* (Table S4). Some of these genes are known cell cycle regulators in HSCs (Rossi et al., 2012; Tesio and Trumpp, 2011). Surprisingly, we also noticed that a group of genes involved in immune responses and inflammation, comprising *Cfp* (Properdin), *Socs2*, *Ccr1*, *Ccr2*, *Ccr5*, *Chga* (Chromogranin A), *Ifi30* (Interferon Gamma-Inducible Protein 30), *Lgmn*, *Txn*, and *Sell* (selectin L), were upregulated in *Fancd2*⁻/⁻ KSL cells (Tables 1 and S4).

Changes in mRNA Expression Profile in HSPCs in Response to OXM Administration Reveal a Mechanism behind OXM's Proliferation-Stimulating Effect

In order to interrogate the mechanism underlying the cell cycle changes induced by OXM, we performed RNA-Seq on HSPCs from the placebo and OXM treatment groups. Considering that the proliferation-enhancing effect of OXM was observed in both *Fancd2* mutant and WT mice, we focused our analysis on OXM-altered genes shared by both genotypes. Only four genes (Table 2) changed their expression levels significantly after OXM administration in both *Fancd2*⁻/⁻ and WT mice. Both *mKi67* and *Cenpf* are cell cycle-regulated genes and proliferation markers.
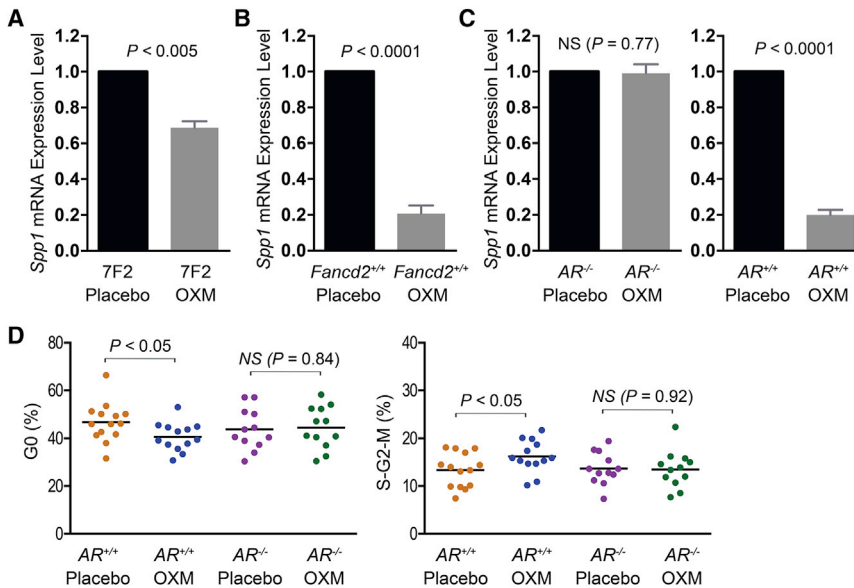
In fact, the *mKi67*-encoded protein is the antigen recognized by anti-KI67 antibody, the same antibody used in our cell cycle analysis. The RNA-Seq data demonstrated that both genes were expressed at lower levels in KSL cells, as compared with whole bone marrow cells, and were mildly but significantly upregulated after OXM administration, further confirming our observation above that OXM stimulates the proliferation of HSPCs in both *Fancd2*⁻/⁻ and WT mice.

Two genes, *Spp1* and *Oasl2*, were significantly downregulated after OXM administration. *Spp1* in particular was affected and was suppressed over 10-fold (Table 2). *Spp1* was expressed at similar levels in both HSPCs and whole bone marrow cells (Table S3) and encodes secreted phosphoprotein 1 (also known as osteopontin), a cytokine known to upregulate the expression of certain interferons and interleukins. The other gene *Oasl2* was enriched 11-fold in HSPCs compared with whole bone marrow cells (Table S3). *Oasl2* encodes 2′-5′ oligoadenylate synthetase-like 2 and belongs to a highly conserved family of interferon-induced enzymes (Hovanessian and Justesen, 2007). Since both genes are known to inhibit proliferation (Kumar and Mendelsohn, 1989; Nilsson et al., 2005), it is plausible that OXM-mediated suppression of these genes underlies its proliferation-promoting effects.

It is worth noting that no expression changes in *mTert* RNA expression levels were detected in response to OXM administration (Table S5), although *mTert* mRNA was enriched 13-fold in HSPCs of both *Fancd2*⁻/⁻ and WT mice (Table S3). Therefore, the induction of telomerase (Calado et al., 2009) is unlikely to underlie the activity of OXM during chronic administration.

OXM Suppresses Spp1 Transcription in an Androgen Receptor-Dependent Manner

Although it has never been reported that *Spp1* is an androgen-target gene, a genome-wide profiling of androgen receptor (AR) binding identified one AR target site in intron 3

Figure 5. OXM Suppresses *Spp1* Transcription through the Mediation of AR

(A) OXM suppressed *Spp1* gene expression in cultured 7F2 mouse osteoblasts. RNA input was normalized based on glyceraldehyde 3-phosphate dehydrogenase mRNA expression. The *Spp1* expression level in placebo-treated 7F2 cells was set at 1 as a reference. Data are pooled results from four independent experiments. Data are presented as mean ± SEM.

(B) OXM suppressed *Spp1* gene expression in kidneys. Data are pooled results from multiple female mice (n = 4 for each group).

(C) *Spp1* gene expression levels were not suppressed by OXM in the kidneys of AR-deficient mice. Data are pooled results from multiple female mice (n = 3 for each group).

(D) OXM stimulated KSL cell proliferation through the mediation of AR. Data are pooled results from multiple mice (n = 14 for placebo $AR^{+/+}$ group, n = 13 for OXM $AR^{+/+}$ group, and n = 12 for either OXM or placebo group of $AR^{-/-}$ mice). NS denotes not significant.

See also Figures S4 and S5 and Table S6.

of the human *SPP1* gene (Figure S4A) (Massie et al., 2011). Bioinformatics analysis using UCSC PhyloP basewise conservation tool (http://genome.ucsc.edu/) further revealed that this AR target site was highly conserved across different species (Figure S4B). Furthermore, a BLAT search with the human AR target sequence returned an intronic sequence with 84% DNA sequence identity in the mouse *Spp1* gene. The *Spp1*-encoded osteopontin is known to be produced by osteoclasts and osteoblasts (Nilsson et al., 2005; Stier et al., 2005), but is also expressed in some soft tissues such as the kidney (Hsieh et al., 2006). Since osteoblasts are difficult to purify from bone marrow, we tested *Spp1* transcriptional changes by quantitative RT-PCR in cultured 7F2 mouse osteoblasts in vitro. As shown in Figure 5A, 24 hr of treatment with OXM significantly reduced *Spp1* mRNA level in osteoblasts (p < 0.005). We also measured *Spp1* gene expression levels in vivo by quantitative RT-PCR. As shown in Figure 5B, *Spp1* mRNA levels in the kidneys of chronic OXM-treated mice were 80% lower than those in placebo-treated, gender-matched controls (p < 0.0001). Immunohistochemistry staining of bone sections with an anti-Spp1 antibody confirmed the downregulation of Spp1 in the bone samples from OXM-treated mice (Figure S4C).

Moreover, the suppression of *Spp1* transcription by OXM was dependent on the AR. *Spp1* mRNA levels were unchanged by OXM treatment in AR-deficient mice of C57BL/6J strain background (p = 0.77; Figure 5C). In contrast, WT mice of the same strain showed clear OXM-mediated suppression of *Spp1* transcription (p < 0.0001; Figure 5C).

To further understand the correlation between *Spp1* mRNA levels and HSPC proliferation, we then treated AR-deficient mice with OXM for 4 months and examined the cell cycle profiles of their KSL cells. 44.5% (±2.6%) of KSL cells in OXM-treated $AR^{-/-}$ mice were in the G0 stage of the cell cycle, similar to 43.8% (±2.5%) observed in placebo-treated $AR^{-/-}$ mice (p = 0.84; Figure 5D). Similarly, the proportions of KSL cells in S-G2-M phase in both OXM-treated and placebo-treated $AR^{-/-}$ mice were at the same levels (p = 0.92; Figure 5D). In contrast, in WT control mice of the same C57BL/6J background, significant loss of quiescence and enhanced cycling in OXM-treated group (p < 0.05; Figure 5D) were seen. Taken together, these results suggest that OXM stimulates HSPC proliferation through AR-mediated transcriptional suppression of *Spp1*.

Changes in mRNA Expression Profile in Basophilic Erythroblasts in Response to OXM Rule Out an EPO-Mediated Mechanism of Action by OXM

Finally, we sought to test the previously proposed hypothesis that OXM might activate the EPO pathway in early erythroid progenitors to enhance erythropoiesis (Chute et al., 2010). A group of WT mice was injected with EPO for 3 consecutive days. Complete blood count analysis revealed that the mice on EPO treatment showed higher hemoglobin, an effect similar to that of OXM (Figure S5A). However, the EPO-treated mice also had higher MCV levels

than the placebo-treated controls, a known phenomenon caused by the shift of large, immature reticulocytes into circulation as a consequence of EPO-stimulated stress erythropoiesis (Finch, 1982). The macrocytosis effect from EPO was in clear contrast to OXM's ability to alleviate macrocytosis under our experimental conditions, suggesting a divergence between the two drugs' mechanisms of action in promoting erythropoiesis.

In addition, the serum levels of EPO in mice on OXM or placebo were measured, and no difference was found (Figure S5B), further indicating that OXM did not function through the activation of the EPO pathway.

In order to further understand this issue and identify any potential targets of OXM in erythroid progenitors, we next sorted TER119^{high}/CD71^{high}/FSC^{high} basophilic erythroblasts by flow cytometry and investigated the differential mRNA expression profiles with and without OXM administration in WT mice. Basophilic erythroblasts were chosen because this population expresses abundant Epo receptor (Singbrant et al., 2011). OXM had no effect on the abundance of this population (data not shown). No significant differences at all in gene expression were found between OXM-treated WT erythroid progenitors and their placebo-treated counterparts, with no gene displaying an expression change higher than 1.2-fold. Importantly, no upregulation of EPO-inducible genes such as *Socs1*, *Socs2*, *Socs3*, and *Cish* (Ingley, 2012) was seen in WT mice treated with OXM (Table S6). In addition, there was no differential expression of the well-known EPO target transferrin receptor or any other major players of the Epo-R signaling network such as *Bcl2l1*, *Cdc25a*, *Btg3*, *Ccnd2*, *Lyl1*, *Pim3*, and *Tnfrsf13c* (Singh et al., 2012) (Table S6). These results further confirm that EPO does not play a role in the action of OXM in the erythroid lineage.

It is also important to mention that *Spp1* mRNA expression was undetectable in basophilic erythroblasts (Table S7), whereas it was robustly expressed in HSPCs.

DISCUSSION

Although OXM has been used for patients with aplastic anemia including FA for many years, its mechanism of action remains poorly understood. The studies described herein provide significant information on how this widely used drug affects hematopoiesis and exerts therapeutic benefit. We found that OXM significantly reduced quiescence and promoted proliferation in KSL hematopoietic stem/progenitor cells. This effect was not specific to FA HSPCs, but affected WT mice just as strongly. The percentage of actively cycling cells increased by at least 50% in both genotypes. Interestingly, the effect of OXM on the cell cycle was specific only to HSPC in both mutant mice

and controls. Other hematopoietic lineages in the bone marrow did not divide more frequently in response to the drug. This finding indicates that OXM administration has a direct effect on the HSPC compartment and is consistent with the fact that the drug is known to increase the numbers of all blood lineages in humans, including red blood cells, platelets, and neutrophils (Shimamura and Alter, 2010). Although the HSPCs clearly cycle more rapidly on OXM, the number of immunophenotypically defined stem cells did not increase in either mutants or WT mice. This suggests that the newly generated cells rapidly feed into the progenitor compartment rather than generating new stem cells by self-renewal. In fact, our data show that chronic OXM administration eventually results in stem cell exhaustion. The long-term repopulating ability of stem cells from OXM-treated mice was significantly lower than those of placebo-treated controls. This was not unexpected, given the fact that multiple genetic mutations associated with reduced stem cell quiescence have been shown to result in eventual stem cell depletion (Orford and Scadden, 2008). We have previously shown that FA HSPCs already have an accelerated cell cycle and interpreted this finding as a homeostatic mechanism that compensates for the increased loss of stem cells in this disease (Zhang et al., 2010). The administration of OXM can further enhance this compensatory mechanism, at least temporarily, and indeed does improve multiple hematological parameters in FA mice. However, our data predict that OXM will not provide a permanent rescue of hematopoiesis and that a more definitive method of treatment will be eventually needed, even in good early responders. In fact, many FA patients eventually become androgen resistant even if their initial response was positive (Shimamura and Alter, 2010). It is possible that HSCs in these patients have been completely depleted at later stage of the treatment.

The analysis of the transcriptome of OXM-treated HSPCs was revealing. First, the data showed very clearly that the mRNA levels of *mTERT* were not different between treated and untreated animals. In vitro studies by others have shown that OXM can enhance telomerase activity through estrogen receptor-mediated signaling in short-term assays (Calado et al., 2009). However, this effect was not observed in the long-term in vivo studies described herein. Furthermore, enhanced expression of telomerase, even if present, would not explain the observed effect on stem cell quiescence. We conclude that increased telomerase activity is not the primary mechanism by which OXM acts in vivo. Second, the RNA expression data confirmed that the cell cycle was changed by OXM at the transcriptional level. For example, the mRNA encoding the KI67 antigen was clearly induced. More importantly, however, the data demonstrated a profound (~10-fold) decrease in osteopontin mRNA. This effect of OXM on osteopontin

transcription was AR dependent and likely mediated directly by an AR-target site in *Spp1* gene. This finding has clinical implications because it indicates that the use of AR antagonists (Gao, 2010) is not a viable strategy to ameliorate the masculinizing side effects of androgens in bone marrow failure patients.

Although osteopontin is best known as a protein found in bone (Nilsson et al., 2005; Stier et al., 2005), it is expressed at robust levels in the stem cells themselves, as evidenced by our RNA-Seq analysis of KSL cells and previously published gene expression database on SPKSL cells (Chambers et al., 2007) (Figure S6). Its precise function in HSPCs is unclear, but it has been shown that *Spp1*$^{-/-}$ stem cells have an accelerated cell cycle (Nilsson et al., 2005). It has generally been thought that osteopontin expressed by bone cells in the HSC niche acts on stem cells in a paracrine mode (Nilsson et al., 2005; Stier et al., 2005). Our data indicate that this protein may also have a cell autonomous effect in stem cells. Future studies with cell-type specific knockouts will be required to address this hypothesis. A second gene, *Oasl2,* was also suppressed by OXM. *Oasl2* (2′-5′ oligoadenylate synthetase-like 2), has not been well studied in HSPCs, despite its known high expression in hematopoietic tissues (Hartmann et al., 1998; Tiefenthaler et al., 1999). Our RNA-Seq data further showed that *Oasl2* expression was 11-fold higher in KSL cells than that in whole bone marrow cells. Several publications have identified its proapoptotic and antiproliferative roles in other cell types (Ghosh et al., 2001; Kumar and Mendelsohn, 1989), but its high expression level in KSL cells suggests that it might have a direct role in HSPC function. As a cytokine, osteopontin upregulates the expression of interferons and interleukins. Conversely, *Oasl2* is known to be induced by interferons (Hovanessian and Justesen, 2007), promote apoptosis, and suppress proliferation (Ghosh et al., 2001; Kumar and Mendelsohn, 1989). Collectively, it is tempting to speculate that osteopontin and 2′-5′ oligoadenylate synthetase-like 2 function in the same pathway to inhibit HSPC proliferation. OXM's primary mode of action would be to transcriptionally repress this growth inhibitory pathway.

Many publications have suggested that overexpression of osteopontin may play a role in the biology of some cancers, including acute myelogenous leukemia (Bandopadhyay et al., 2014; Liersch et al., 2012), and that its suppression could be therapeutically beneficial. Our data suggest that OXM or other androgens could readily be used for this purpose. OXM should be tested in preclinical animal models of relevant tumors to determine whether it impairs tumor growth.

Our results also shed light on another hypothesis regarding the mechanism of action of androgens in anemia. Early work suggested that androgens stimulate erythropoiesis via the activation of EPO pathway. However, subsequent studies found no correlation between serum EPO and androgen levels (Chute et al., 2010). Similarly, we also observed no difference in serum EPO levels between OXM- and placebo-treated mice, despite finding a substantial increase in renal mass in OXM-treated mice, a phenomenon well known to be associated with chronic androgen administration (Shukla et al., 1992). Consistent with this, RNA-Seq transcriptome analysis of early erythroid progenitors did not show any induction of critical EPO-inducible genes or EPO target genes after OXM treatment. Moreover, under our experimental conditions, OXM reduced the MCV level whereas EPO causes macrocytosis, indicating a clear divergence between the action of the two. Our data therefore argue strongly against an EPO-mediated mechanism of action for androgen therapy.

Our data also provide information on the pathophysiology of FA itself. First, we found that the drastic acceleration of cell cycling observed in *Fancd2*$^{-/-}$ HSPCs is unique to this blood cell population. No cell cycle abnormalities were observed in mature hematopoietic lineages. Others have found that the hypersensitivity of FA cells to acetaldehyde is also uniquely limited to HSPCs (Garaycoechea et al., 2012) and that it is possible that the lack of stem cell quiescence is mediated by aldehyde toxicity. Unfortunately, OXM had no effect on the expression of any aldehyde-detoxifying genes in stem cells, including *Aldh2*. Second, in the past, FA mouse models have been considered to be poor models of the human disease because they did not develop readily detectable anemia. Our results, however, indicate that *Fancd2*$^{-/-}$ mice actually recapitulate the disease rather faithfully when the animals are observed for a longer time period commensurate with the time it takes to develop anemia in humans. We observed clear declines in platelet counts, obvious red cell abnormalities, including macrocytosis, and even osteopetrosis. We also found that OXM therapy had similar effects to those reported in human FA patients, improving platelet counts, red blood cell counts, and hemoglobin levels, with no changes in white blood cell counts. Overall, we conclude that aged *Fancd2*$^{-/-}$ mutant mice are an adequate model for spontaneous bone marrow failure and can be used for preclinical drug efficacy studies.

Finally and most importantly, we found critical gene expression changes in HSPCs of *Fancd2* mutant mice. The changes in cell cycle-related genes and genes involved in DNA damage responses were not surprising, given the obvious lack of stem cell quiescence and the known role of the FA pathway in DNA repair (Kim and D'Andrea, 2012). However, we also found significant changes in multiple genes involved in immune responses. Recent work has clearly shown that DNA damage can activate innate immunity (Gasser et al., 2005) by signals emanating from the

damaged cell. Abnormalities in cytokine sensitivity and cytokine levels have long been known to be present in FA (Nalepa and Clapp, 2014). We therefore hypothesize that some genes upregulated in FA HSPCs may be part of an innate immune response to DNA damage. In this model, DNA damage-mediated signals originating from stem cells eventually activate systemic inflammation and cytokine elevations. These proinflammatory cytokines can be toxic to stem cells and cause further genomic damage, thus creating a vicious circle resulting in bone marrow failure.

EXPERIMENTAL PROCEDURES

Mice

Fancd2 mutant, *Fancc* mutant, and *ROSA26* transgenic mice were maintained on the 129S4 strain background as described before (Zhang et al., 2010). $AR^{-/-}$ mice were originally developed in Dr. Kato's lab and maintained on the C57BL/6J background (Shiina et al., 2006). OXM was obtained from Sigma, milled into standard rodent chow at 300 mg/kg diet (Bio-Serv), and given to the mice upon weaning (3–4 weeks of age). For complete blood count and KSL frequency analyses, the treatment continued for 17 months until harvest. For cell cycle analysis and OXM biological activity, the treatment continued for 4 months; for RNA extraction, the treatment continued for 3 months. Recombinant human EPO (Procrit from Amgen) was given in three consecutive doses at 3,000 IU on day 1, 1,000 IU on day 2, and day 3. All animals were treated in accordance with the guidelines of the Institutional Animal Care and Use Committee.

Cell Culture

7F2 mouse osteoblast (ATCC CRL-12557) cells were purchased from ATCC. For in vitro OXM treatment, cells were split at the ratio of 1:10 and plated with 5 μM OXM-supplemented medium. Twenty-four hours later, cells were harvested for RNA isolation with Trizol reagent.

Complete Blood Count

Complete blood counts were measured by IDEXX Laboratories to monitor hematological parameters.

Histopathology

Bone marrow smears and peripheral blood smears were stained with Wright-Giemsa Stain (Polysciences).

Flow Cytometry

Flow cytometry experiments were performed as described previously (Zhang et al., 2010). Propidium iodide was included as a viability dye. Mouse IgG1 isotype control (for cell cycle analysis) or fluorescence minus one controls (in all the other cases) were used for gating. Cytometric data were analyzed using FlowJo software v.9.6.1 (Tree Star).

Fractionation of erythroblasts at various stages of differentiation in bone marrow was achieved by combining cell surface marker staining of CD71 and TER119 with the analysis of cell size (based on flow cytometric forward scatter intensity) (Singbrant et al., 2011). Bone marrow cells were stained with FITC-conjugated anti-mouse CD71 and PE-Cy7-conjugated antimouse TER119. The TER119^{high}/CD71^{high}/FSC^{high} basophilic erythroblast fraction was sorted on a Cytopeia Influx cell sorter equipped with four lasers, allowing for excitation wavelengths of 355, 488, 561, and 633 nm.

Competitive Repopulation Assay

Whole bone marrow cells were isolated from OXM- or placebo-treated mice. After red cell lysis, nucleated cells were counted and mixed with competing *ROSA26* bone marrow cells for transplantation. *Fancd2*$^{-/-}$ cells were mixed with *ROSA26* cells at a 3:1 ratio, whereas *Fancd2*$^{+/+}$ cells were mixed with *ROSA26* at 1:1 ratio. A total of 4 million mixed cells was used for retro-orbital injection of each recipient *Fancc*$^{-/-}$ mouse preconditioned with a split whole-body lethal dose of 12 Gy irradiation (6 Gy each, 4 hr apart). Six months after transplantation, DNA was extracted for quantitative real-time PCR analysis, and each original donor's contribution to peripheral blood was calculated to assess peripheral blood chimerism. PCR primers were listed in Table S8.

RNA-Seq

RNA was extracted using Trizol reagent (Invitrogen), followed by RNAeasy Mini Kit (QIAGEN) and DNase I treatment. RNA quality was determined by an Agilent 2100 Bioanalyzer (Agilent technology). Three samples per condition were processed to ensure sufficient power for detecting any differentially expressed genes. For KSL libraries, each sample represented total mRNA isolated from pooled KSL cells of five individual mice; for basophilic erythroblast libraries, each library represented total mRNA isolated from basophilic erythroblasts of one individual mouse.

Libraries were constructed using TruSeq RNA Sample Preparation Kit (Illumina) according to the manufacturer's instructions and sequenced as 51 base-length reads using Illumina HiSeq 2000 genome analyzer. All reads were mapped to the mouse reference genome (version mm 9) using Bowtie short read aligner software (http://bowtie-bio.sf.net). Data analysis was performed using EdgeR GLM algorithms (McCarthy et al., 2012). Data mining and pathway analysis were carried out with the MetaCore integrated software suite (Thomson Reuters).

Serum EPO Test

Serum samples were tested for EPO levels using a mouse EPO-specific ELISA at Ani Lytics.

Statistical Analyses

Two-tailed, unpaired Student's t tests were performed to calculate p values using Prism 6.0c software (GraphPad Software). A p value less than 0.05 was considered significant.

ACCESSION NUMBERS

The RNA-Seq raw data have been deposited into GEO (Gene Expression Omnibus), a public functional genomics data repository at NCBI. The accession number is GSE58724.

REFERENCES

Bandopadhyay, M., Bulbule, A., Butti, R., Chakraborty, G., Ghorpade, P., Ghosh, P., Gorain, M., Kale, S., Kumar, D., Kumar, S., et al. (2014). Osteopontin as a therapeutic target for cancer. Expert Opin. Ther. Targets 18, 883–895.

Calado, R.T., Yewdell, W.T., Wilkerson, K.L., Regal, J.A., Kajigaya, S., Stratakis, C.A., and Young, N.S. (2009). Sex hormones, acting on the TERT gene, increase telomerase activity in human primary hematopoietic cells. Blood 114, 2236–2243.

Chambers, S.M., Boles, N.C., Lin, K.Y., Tierney, M.P., Bowman, T.V., Bradfute, S.B., Chen, A.J., Merchant, A.A., Sirin, O., Weksberg, D.C., et al. (2007). Hematopoietic fingerprints: an expression database of stem cells and their progeny. Cell Stem Cell 1, 578–591.

Chute, J.P., Ross, J.R., and McDonnell, D.P. (2010). Minireview: Nuclear receptors, hematopoiesis, and stem cells. Mol. Endocrinol. 24, 1–10.

Crossan, G.P., van der Weyden, L., Rosado, I.V., Langevin, F., Gaillard, P.H., McIntyre, R.E., Gallagher, F., Kettunen, M.I., Lewis, D.Y., Brindle, K., et al.; Sanger Mouse Genetics Project (2011). Disruption of mouse Slx4, a regulator of structure-specific nucleases, phenocopies Fanconi anemia. Nat. Genet. 43, 147–152.

Dokal, I. (2003). Inherited aplastic anaemia. Hematol. J. 4, 3–9.

Finch, C.A. (1982). Erythropoiesis, erythropoietin, and iron. Blood 60, 1241–1246.

Gao, W. (2010). Androgen receptor as a therapeutic target. Adv. Drug Deliv. Rev. 62, 1277–1284.

Garaycoechea, J.I., Crossan, G.P., Langevin, F., Daly, M., Arends, M.J., and Patel, K.J. (2012). Genotoxic consequences of endogenous aldehydes on mouse haematopoietic stem cell function. Nature 489, 571–575.

Gasser, S., Orsulic, S., Brown, E.J., and Raulet, D.H. (2005). The DNA damage pathway regulates innate immune system ligands of the NKG2D receptor. Nature 436, 1186–1190.

Ghosh, A., Sarkar, S.N., Rowe, T.M., and Sen, G.C. (2001). A specific isozyme of 2′-5′ oligoadenylate synthetase is a dual function pro-apoptotic protein of the Bcl-2 family. J. Biol. Chem. 276, 25447–25455.

Hartmann, R., Olsen, H.S., Widder, S., Jorgensen, R., and Justesen, J. (1998). p59OASL, a 2′-5′ oligoadenylate synthetase like protein: a novel human gene related to the 2′-5′ oligoadenylate synthetase family. Nucleic Acids Res. 26, 4121–4128.

Houghtaling, S., Timmers, C., Noll, M., Finegold, M.J., Jones, S.N., Meyn, M.S., and Grompe, M. (2003). Epithelial cancer in Fanconi anemia complementation group D2 (Fancd2) knockout mice. Genes Dev. 17, 2021–2035.

Hovanessian, A.G., and Justesen, J. (2007). The human 2′-5′oligoadenylate synthetase family: unique interferon-inducible enzymes catalyzing 2′-5′ instead of 3′-5′ phosphodiester bond formation. Biochimie 89, 779–788.

Hsieh, Y.H., Juliana, M.M., Hicks, P.H., Feng, G., Elmets, C., Liaw, L., and Chang, P.L. (2006). Papilloma development is delayed in osteopontin-null mice: implicating an antiapoptosis role for osteopontin. Cancer Res. 66, 7119–7127.

Ingley, E. (2012). Integrating novel signaling pathways involved in erythropoiesis. IUBMB Life 64, 402–410.

Kim, H., and D'Andrea, A.D. (2012). Regulation of DNA cross-link repair by the Fanconi anemia/BRCA pathway. Genes Dev. 26, 1393–1408.

Kumar, R., and Mendelsohn, J. (1989). Role of 2′-5′-oligoadenylate synthetase in gamma-interferon-mediated growth inhibition of A431 cells. Cancer Res. 49, 5180–5184.

Kutler, D.I., Singh, B., Satagopan, J., Batish, S.D., Berwick, M., Giampietro, P.F., Hanenberg, H., and Auerbach, A.D. (2003). A 20-year perspective on the International Fanconi Anemia Registry (IFAR). Blood 101, 1249–1256.

Levillain, O., Diaz, J.J., Blanchard, O., and Déchaud, H. (2005). Testosterone down-regulates ornithine aminotransferase gene and up-regulates arginase II and ornithine decarboxylase genes for polyamines synthesis in the murine kidney. Endocrinology 146, 950–959.

Liersch, R., Gerss, J., Schliemann, C., Bayer, M., Schwöppe, C., Biermann, C., Appelmann, I., Kessler, T., Löwenberg, B., Büchner, T., et al. (2012). Osteopontin is a prognostic factor for survival of acute myeloid leukemia patients. Blood 119, 5215–5220.

Massie, C.E., Lynch, A., Ramos-Montoya, A., Boren, J., Stark, R., Fazli, L., Warren, A., Scott, H., Madhu, B., Sharma, N., et al. (2011). The androgen receptor fuels prostate cancer by regulating central metabolism and biosynthesis. EMBO J. 30, 2719–2733.

McCarthy, D.J., Chen, Y., and Smyth, G.K. (2012). Differential expression analysis of multifactor RNA-Seq experiments with respect to biological variation. Nucleic Acids Res. 40, 4288–4297.

Nalepa, G., and Clapp, D.W. (2014). Fanconi anemia and the cell cycle: new perspectives on aneuploidy. F1000Prime Rep. 6, 23.

Nilsson, S.K., Johnston, H.M., Whitty, G.A., Williams, B., Webb, R.J., Denhardt, D.T., Bertoncello, I., Bendall, L.J., Simmons, P.J.,

and Haylock, D.N. (2005). Osteopontin, a key component of the hematopoietic stem cell niche and regulator of primitive hematopoietic progenitor cells. Blood *106*, 1232–1239.

Orford, K.W., and Scadden, D.T. (2008). Deconstructing stem cell self-renewal: genetic insights into cell-cycle regulation. Nat. Rev. Genet. *9*, 115–128.

Parmar, K., Kim, J., Sykes, S.M., Shimamura, A., Stuckert, P., Zhu, K., Hamilton, A., Deloach, M.K., Kutok, J.L., Akashi, K., et al. (2010). Hematopoietic stem cell defects in mice with deficiency of Fancd2 or Usp1. Stem Cells *28*, 1186–1195.

Pulliam-Leath, A.C., Ciccone, S.L., Nalepa, G., Li, X., Si, Y., Miravalle, L., Smith, D., Yuan, J., Li, J., Anur, P., et al. (2010). Genetic disruption of both Fancc and Fancg in mice recapitulates the hematopoietic manifestations of Fanconi anemia. Blood *116*, 2915–2920.

Rossi, L., Lin, K.K., Boles, N.C., Yang, L., King, K.Y., Jeong, M., Mayle, A., and Goodell, M.A. (2012). Less is more: unveiling the functional core of hematopoietic stem cells through knockout mice. Cell Stem Cell *11*, 302–317.

Shiina, H., Matsumoto, T., Sato, T., Igarashi, K., Miyamoto, J., Takemasa, S., Sakari, M., Takada, I., Nakamura, T., Metzger, D., et al. (2006). Premature ovarian failure in androgen receptor-deficient mice. Proc. Natl. Acad. Sci. USA *103*, 224–229.

Shimamura, A., and Alter, B.P. (2010). Pathophysiology and management of inherited bone marrow failure syndromes. Blood Rev. *24*, 101–122.

Shukla, A., Shukla, G.S., and Radin, N.S. (1992). Control of kidney size by sex hormones: possible involvement of glucosylceramide. Am. J. Physiol. *262*, F24–F29.

Singbrant, S., Russell, M.R., Jovic, T., Liddicoat, B., Izon, D.J., Purton, L.E., Sims, N.A., Martin, T.J., Sankaran, V.G., and Walkley, C.R. (2011). Erythropoietin couples erythropoiesis, B-lymphopoiesis, and bone homeostasis within the bone marrow microenvironment. Blood *117*, 5631–5642.

Singh, S., Dev, A., Verma, R., Pradeep, A., Sathyanarayana, P., Green, J.M., Narayanan, A., and Wojchowski, D.M. (2012). Defining an EPOR- regulated transcriptome for primary progenitors, including Tnfr-sf13c as a novel mediator of EPO- dependent erythroblast formation. PLoS ONE *7*, e38530.

Stier, S., Ko, Y., Forkert, R., Lutz, C., Neuhaus, T., Grünewald, E., Cheng, T., Dombkowski, D., Calvi, L.M., Rittling, S.R., and Scadden, D.T. (2005). Osteopontin is a hematopoietic stem cell niche component that negatively regulates stem cell pool size. J. Exp. Med. *201*, 1781–1791.

T'Sjoen, G.G., Beguin, Y., Feyen, E., Rubens, R., Kaufman, J.M., and Gooren, L. (2005). Influence of exogenous oestrogen or (anti-) androgen administration on soluble transferrin receptor in human plasma. J. Endocrinol. *186*, 61–67.

Tesio, M., and Trumpp, A. (2011). Breaking the cell cycle of HSCs by p57 and friends. Cell Stem Cell *9*, 187–192.

Tiefenthaler, M., Marksteiner, R., Neyer, S., Koch, F., Hofer, S., Schuler, G., Nussenzweig, M., Schneider, R., and Heufler, C. (1999). M1204, a novel 2′,5′ oligoadenylate synthetase with a ubiquitin-like extension, is induced during maturation of murine dendritic cells. J. Immunol. *163*, 760–765.

Wang, Z., Gerstein, M., and Snyder, M. (2009). RNA-Seq: a revolutionary tool for transcriptomics. Nat. Rev. Genet. *10*, 57–63.

Zhang, Q.S., Marquez-Loza, L., Eaton, L., Duncan, A.W., Goldman, D.C., Anur, P., Watanabe-Smith, K., Rathbun, R.K., Fleming, W.H., Bagby, G.C., and Grompe, M. (2010). Fancd2-/- mice have hematopoietic defects that can be partially corrected by resveratrol. Blood *116*, 5140–5148.

Zhang, Q.S., Watanabe-Smith, K., Schubert, K., Major, A., Sheehan, A.M., Marquez-Loza, L., Newell, A.E., Benedetti, E., Joseph, E., Olson, S., and Grompe, M. (2013). Fancd2 and p21 function independently in maintaining the size of hematopoietic stem and progenitor cell pool in mice. Stem Cell Res. (Amst.) *11*, 687–692.

Oxymetholone Therapy of Fanconi Anemia Suppresses Osteopontin Transcription and Induces Hematopoietic Stem Cell Cycling

Qing-Shuo Zhang, Eric Benedetti, Matthew Deater, Kathryn Schubert, Angela Major, Carl Pelz, Soren Impey, Laura Marquez-Loza, R. Keaney Rathbun, Shigeaki Kato, Grover C. Bagby, and Markus Grompe

Supplemental Data

Supplementary figure legends:

Figure S1: OXM's bioactivity, related to Figure 2

A). Representative kidney pictures for OXM- or placebo-treated mice. The mice under OXM treatment had larger kidney sizes than their placebo-treated controls. B). OXM-treated mice showed significantly higher kidney weights but maintained similar body weights. Data are pooled results from multiple mice (n = 9 for each group). C). *Oat* gene expression levels in the kidneys of OXM-treated mice were 75% lower than those in placebo-treated gender-matched controls. Data are pooled results from multiple mice (n = 4 for each group).

Figure S2: OXM's effect on the proliferation of LIN⁺ bone marrow cells, related to Figure 4

Representative cell cycle profiles on LIN⁺ cells from OXM-treated mice and their gender-matched placebo-treated littermate controls. For comparison purposes, the profiles were from the same mice used for representative KSL cell cycle profiles shown in Figure 4A. The denoted percentage for each gate was from an individual experiment.

Figure S3: OXM's effect on the proliferation of LIN⁻c-KIT⁺SCA-1⁻ progenitor cells, related to Figure 4

A). Statistical quantification of the cell cycle analysis on LIN⁻c-KIT⁺SCA-1⁻ cells in OXM-treated versus placebo-treated mice. Data represent the mean values from multiple mice (n = 9 for either OXM or placebo group of *Fancd2⁻ᐟ⁻* mice, n = 14 for *Fancd2⁺ᐟ⁺*

placebo group, and n = 10 for *Fancd2*$^{+/+}$ OXM group). B). Representative cell cycle profiles on LIN$^-$c-KIT$^+$SCA-1$^-$ cells from OXM-treated mice and their gender-matched placebo-treated littermate controls. For comparison purposes, the profiles were from the same mice used for representative KSL cell cycle profiles shown in Figure 4A. The denoted percentage for each gate was from an individual experiment.

Figure S4: AR target site in intron 3 of *Spp1* gene, related to Figure 5

A). Sequence of AR target site identified in a previous report (Massie et al., 2011). Note that the authors used human genome assembly version hg18. But the sequence remains the same with latest assembly version hg38. B). Bioinformatics analysis with UCSC PhyloP basewise conservation tool. The AR target site in *Spp1* gene intron 3 was highly conserved across different species. The green arrow indicates this intronic sequence. C). Representative pictures for immunohistochemistry staining of bone sections with anti-Spp1 antibody. Femoral bone sections were stained with anti-osteopontin antibody (R&D Systems, Cat# AF808, 1:100 dilution) and shown in dark brown color. DAPI counterstaining was shown in blue. Original magnification: ×400.

Figure S5: EPO's effects on hematopoiesis, related to Figure 5

A). CBC tests of EPO-treated mice and placebo-treated controls. Data are pooled results from multiple mice (n = 6 for each group). B). Serum EPO levels in OXM-treated mice and placebo-treated controls. Data are pooled results from multiple mice (n = 8 for either OXM or placebo group of *Fancd2*$^{+/+}$ mice, n = 7 for either OXM or placebo group of *Fancd2*$^{-/-}$ mice) and presented as mean ± SEM. NS denotes not significant.
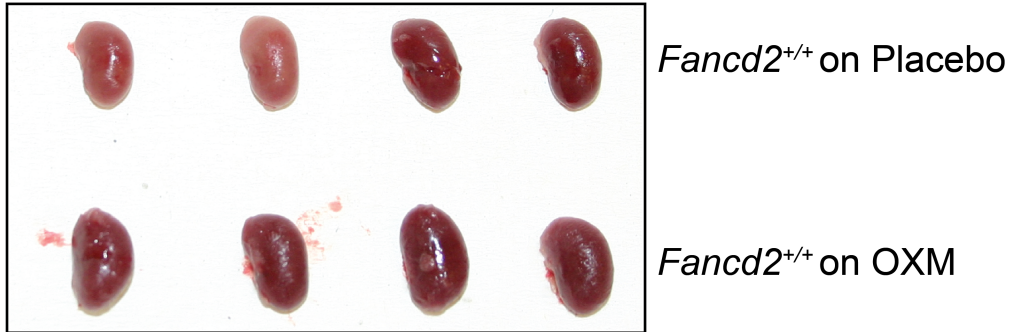
Figure S6: *Spp1* gene expression level in SPKSL cells, related to Table 2

Spp1 gene expression level was from a search result in a previously published gene expression database of SPKSL cells (side population KSL cells, a highly enriched HSC population) (Chambers et al., 2007).
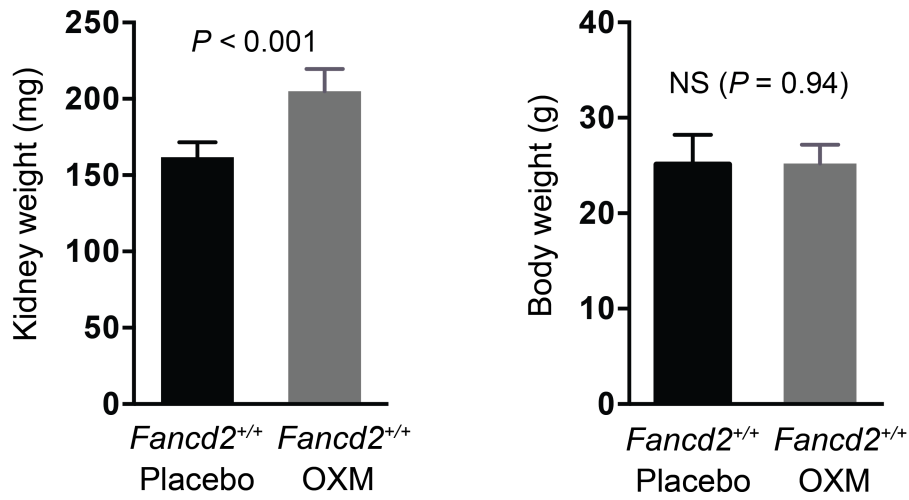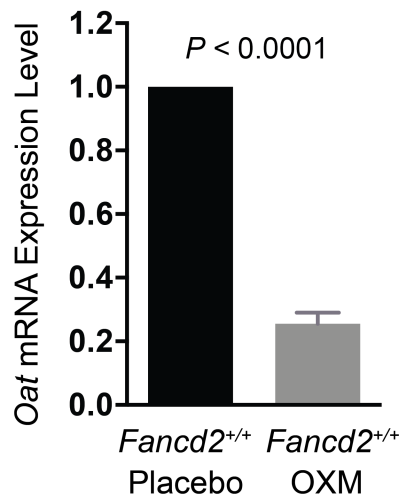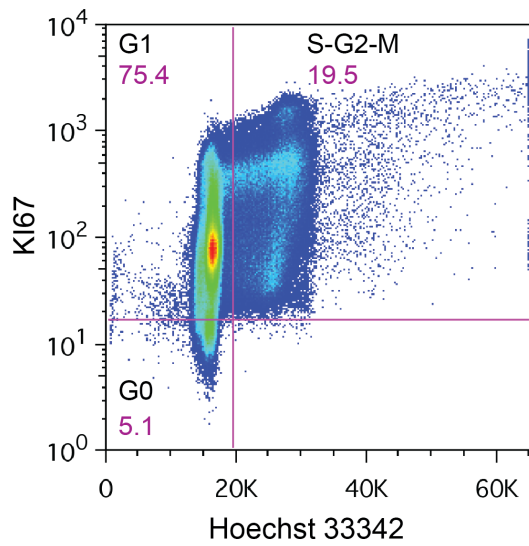
Figure S1

A

Fancd2$^{+/+}$ on Placebo
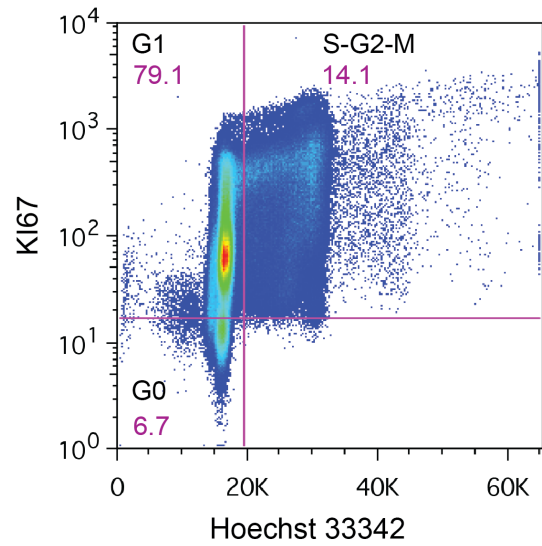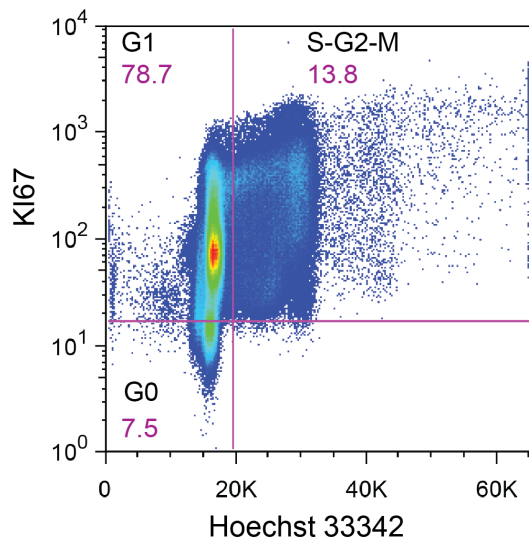
Fancd2$^{+/+}$ on OXM

B

C

Figure S2

Placebo-treated *Fancd2*^{+/+} LIN^{+} cells:

OXM-treated *Fancd2*^{+/+} LIN^{+} cells:

Placebo-treated *Fancd2*^{-/-} LIN^{+} cells:
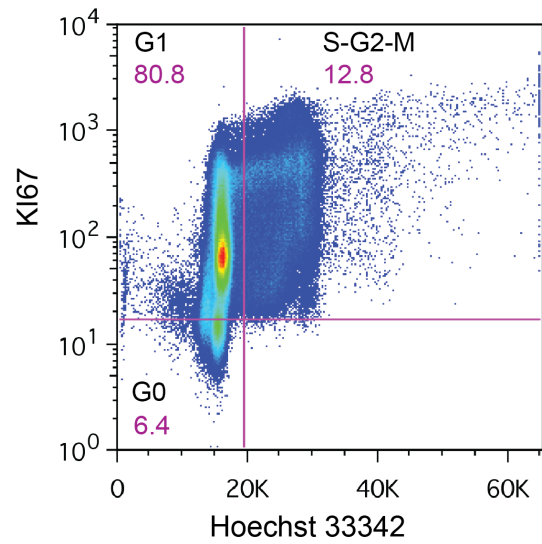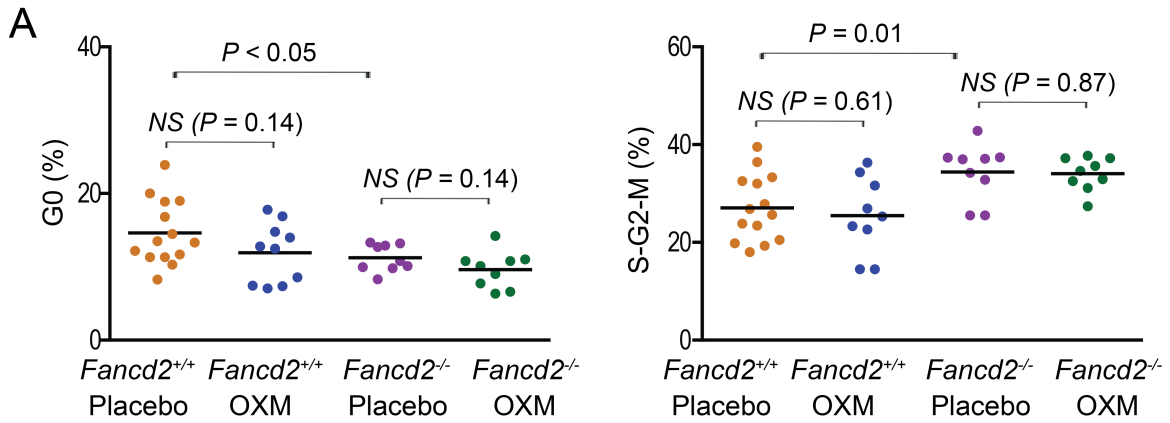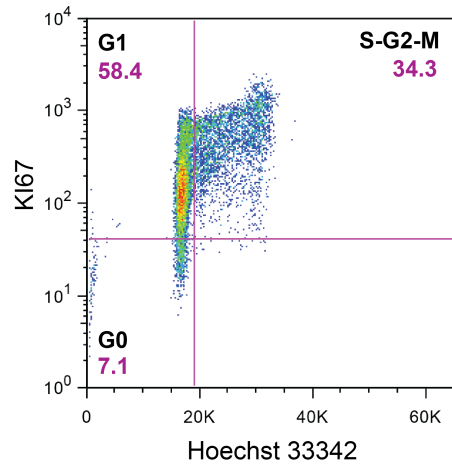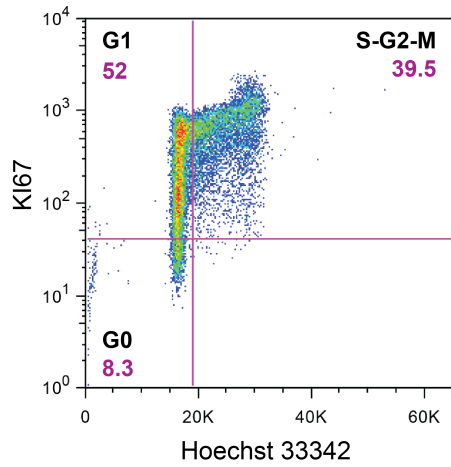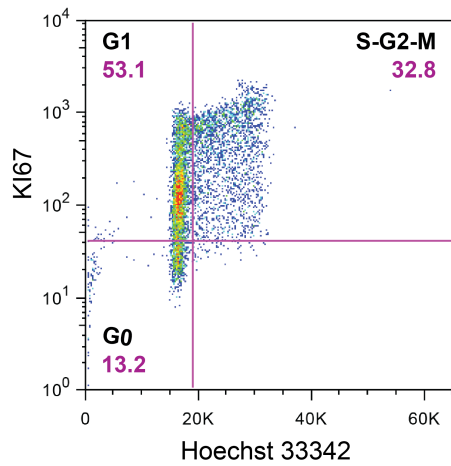

OXM-treated *Fancd2*^{-/-} LIN^{+} cells:

5

Figure S3

A

B

Fancd2⁺/⁺ LIN⁻c-KIT⁺SCA-1⁻ cells / placebo

Fancd2⁺/⁺ LIN⁻c-KIT⁺SCA-1⁻ cells / OXM

Fancd2⁻/⁻ LIN⁻c-KIT⁺SCA-1⁻ cells / placebo
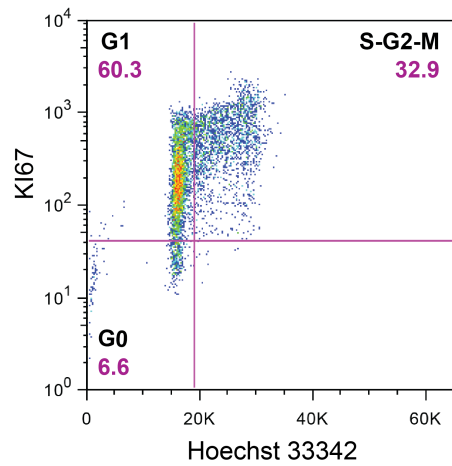
Fancd2⁻/⁻ LIN⁻c-KIT⁺SCA-1⁻ cells / OXM

6

Figure S4

A. AR target site in intron 3 of human *Spp1* gene

```
TGACTGCCTGCTATGAATCTAGGCCAGTACCAAGCACAGTATAGTTTTTAATAAA
TATAAGTTTATAAAACCAACCCAGATATTTTAAATATAATAATATCTAGGCATGT
ATGATGAGTTATCGCATGTAAGATAAGTTATATGAAGTTGTGTGACTTTTTTTCC
ATTAGTCCACATACTGATCTAAAAGCAGAAAATTCCAGCTTTTGCTTTGTTTAGT
GGATTGCTAAGTTTAAAATTCACATTGGATATTAGTCAGAACTGTTTGTATGACC
ATAATATTCACAATATTGTCTGAGATATTAGCTGAGAAGCCCATTGTGAAAAGAA
AGTCTATGTGTGCTGTTTGTATCTATTGTGATTGTCAGCTGATGTTAGATCACAT
TTTCTAACCAAACATAAGACCAACCAAACTCTTTATTATAATTATTTGACCAGCA
CTAAAGATGTACCTACCCCTCCACAACAGATGAAACTGTGCCAGCCAAACAACAA
ATGGGCATTGTCCCCAGAAGCTTGGACAAAAAGGCACACAGAGTTCAATTCCAGT
TGAACAGAATAAAGGCCAAAATAGAGCTGCCTTGGGGGTCACTGCAATTAGACTG
CTTAATGAAGACATTAAAAGAAGTATTCTGTGTTCGTTTGTGTGTGGAGGGGTGT
GTGTGTCTGTTTTTCAACTGATTTGAAAATACAGGTGT
```

B

UCSC Genome Browser on Human Mar. 2006 (NCBI36/hg18) Assembly
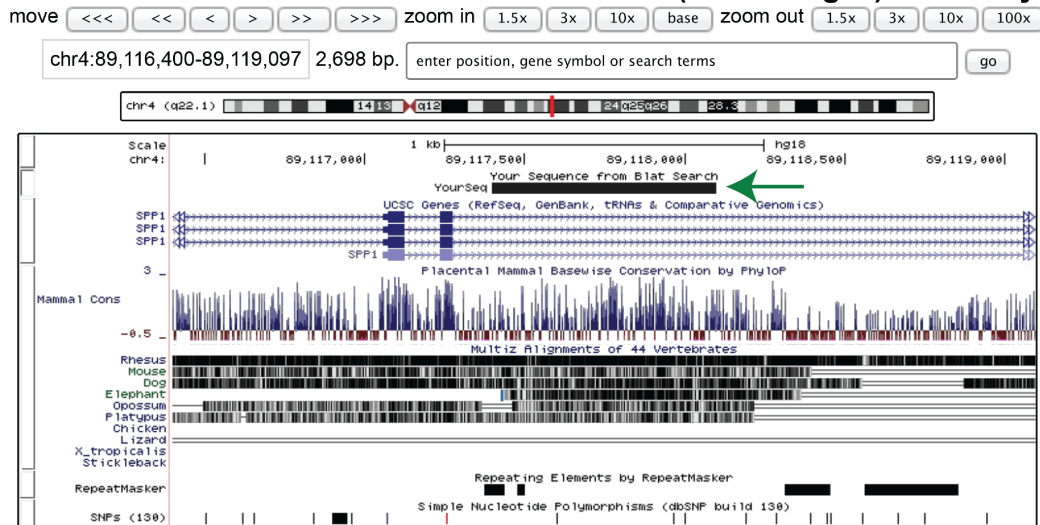
C
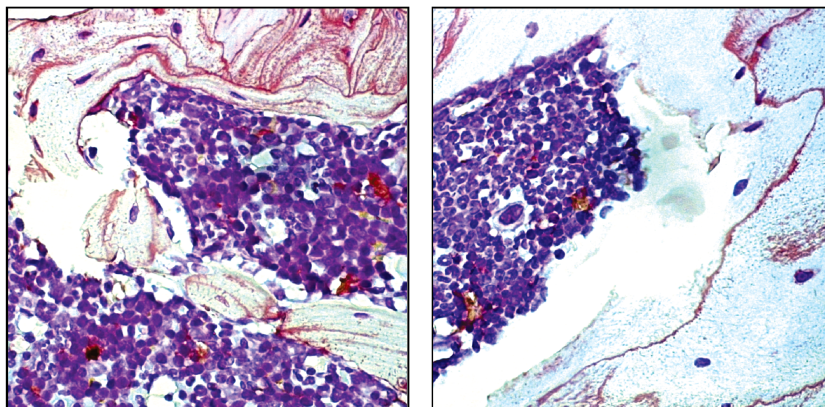
Fancd2-/-   Placebo   *Fancd2*-/-   OXM

Figure S5

A

B

Figure S6:
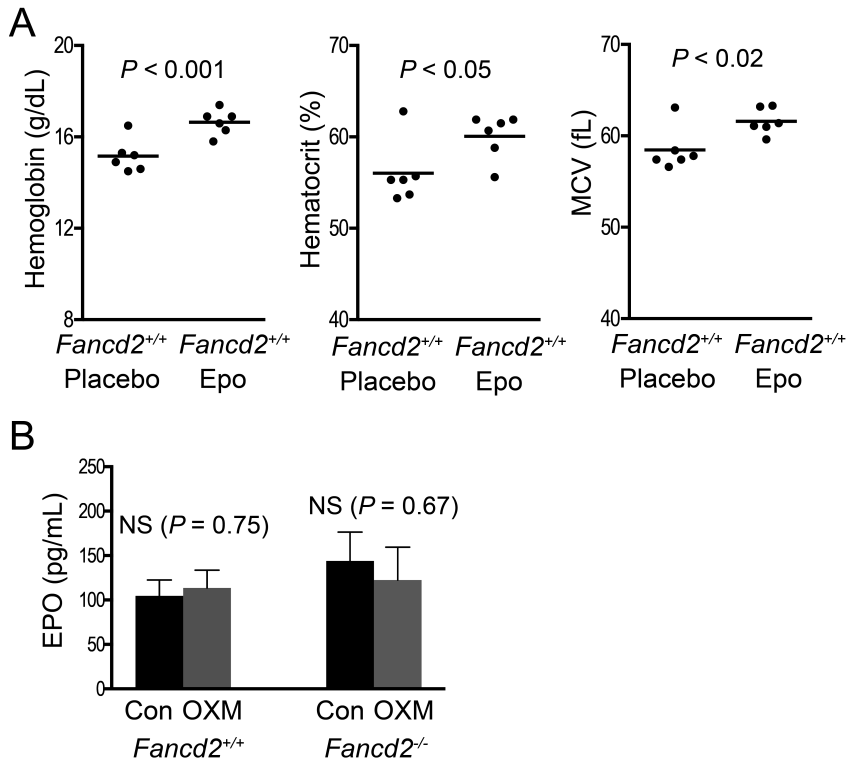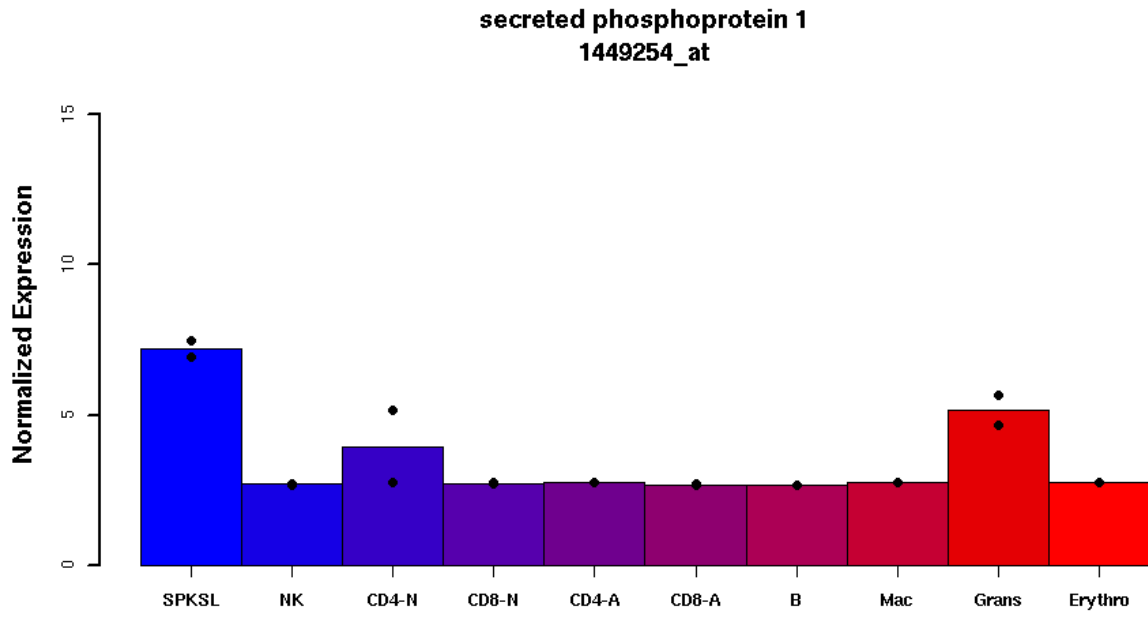

secreted phosphoprotein 1
1449254_at

Supplemental tables

Table S1: Blood counts in young adult *Fancd2$^{-/-}$* and *Fancd2$^{+/+}$* mice, related to Figure 1

	Fancd2$^{+/+}$	*Fancd2$^{-/-}$*	*p*
WBCs, x10^3/μL	6.7 ± 0.5	6.8 ± 0.5	0.92
RBCs, x10^6/μL	10.0 ± 0.1	9.9 ± 0.1	0.38
Hemoglobin, g/dL	14.9 ± 0.1	15.1 ± 0.2	0.25
Hematocrit, %	54.1 ± 0.6	53.8 ± 0.5	0.70
MCV, fL	54.1 ± 0.3	55.1 ± 0.4	0.03
MCH, pg	14.9 ± 0.1	15.4 ± 0.1	0.00
MCHC, %	27.6 ± 0.2	27.9 ± 0.2	0.23
Platelets, x10^3/μL	812 ± 32	643 ± 22	0.00

Comprehensive CBC tests were measured for *Fancd2$^{+/+}$* and *Fancd2$^{-/-}$* mice (4-6 months old, 23 mice in each group) by IDEXX Laboratories. Data were analyzed with Prism 6.0c software and presented as mean value ± SEM.

WBCs denotes white blood cells; RBCs, red blood cells; MCV, mean corpuscular volume; MCH, mean corpuscular hemoglobin; and MCHC, mean corpuscular hemoglobin concentration.

Table S2: mRNA expression changes in *Fancd2$^{-/-}$* KSL cells compared to wild-type KSL cells, related to Table 1

– See the Excel file for Table S2

Table S3: mRNA expression changes in wild-type KSL cells compared to wild-type whole bone marrow cells, related to Table 1

– See the Excel file for Table S3

Table S4: Lists of genes in the important pathways altered in *Fancd2*$^{-/-}$ HSPCs as compared to wild-type HSPCs, related to Table 1

Symbol	RefSeq ID	Gene Name	Change	Q Value
Cell cycle regulation:				
Ccna2	NM_009828	cyclin A2	1.6	0.000
Ccnb1	NM_172301	cyclin B1	2.0	0.000
Ccnb2	NM_007630	cyclin B2	1.8	0.000
Ccnd1	NM_007631	cyclin D1	1.7	0.000
Cdk1	NM_007659	cell division cycle 2 homolog A	1.8	0.000
Cdc25c	NM_009860	cell division cycle 25 homolog C	1.9	0.000
Cdca3	NM_013538	cell division cycle-associated 3	1.7	0.000
Cdkn3	NM_028222	Cyclin-Dependent Kinase Inhibitor 3	1.8	0.003
Cks1b	NM_016904	CDC28 protein kinase subunit 1b	1.6	0.000
Cdca5	NM_026410	cell division cycle-associated 5	1.6	0.000
Cdc45	NM_009862	cell division cycle 45 homolog	1.5	0.000
Ube2c	NM_026785	ubiquitin-conjugating enzyme E2C	2.2	0.000
Nek2	NM_010892	NIMA-related expressed	1.8	0.010
Birc5	NM_001012273	survivin	1.8	0.000
Mad2l1	NM_019499	MAD2-like 1	1.5	0.000
Pttg1	NM_013917	pituitary tumor-transforming 1	2.0	0.000
Aurka	NM_011497	serine/threonine protein kinase 6	1.8	0.000
Inflammatory and immune response:				
Cfp	NM_008823	complement factor properdin	1.6	0.000
Ccr5	NM_009917	chemokine (C-C motif) receptor 5	2.4	0.000
Socs2	NM_007706	suppressor of cytokine signaling 2	2.5	0.000
Chga	NM_007693	chromogranin A	3.5	0.000
Ccr1	NM_009912	chemokine (C-C motif) receptor 1	3.4	0.000
Ccr2	NM_009915	chemokine (C-C motif) receptor 2	1.8	0.000
Ifi30	NM_023065	interferon gamma inducible protein 30	1.8	0.004
Lgmn	NM_011175	legumain	1.6	0.011
Sell	NM_011346	L-selectin	1.8	0.000

Table S5: Differential gene expression of telomerase protein subunit in *Fancd2*$^{-/-}$ or wild-type HSPCs in response to OXM administration, related to Table 2

Genotype	Symbol	Gene ID	Fold change	[c]Q value
Fancd2$^{-/-}$	*Tert*	NM_009354	-1.05	0.27
Wild-type	*Tert*	NM_009354	1.05	0.70

Note: [c]Q value cut-off was set at 0.05.

Table S6: mRNA expression changes of critical EPO-inducible or target genes in wild-type basophilic erythroblasts in response to OXM administration, related to Figure 5

Symbol	RefSeq ID	Con1	Con2	Con3	Oxm1	Oxm2	Oxm3	Q value	AvgFC
Cish	NM_009895	19	29	7	32	13	9	1	n/a
Socs1	NM_009896	4	4	2	2	2	1	1	n/a
Socs2	NM_007706	2	2	2	2	1	0	1	n/a
Socs3	NM_007707	13	6	12	11	2	6	1	n/a
Tfrc	NM_011638	67455	64327	61344	69170	64641	62324	1	1.02
Bcl2ll	NM_009743	6599	4948	6058	5929	5765	6129	1	1.01
Cdc25a	NM_007658	1500	1846	1660	1682	1648	1683	1	1.00
Btg3	NM_009770	0	1	2	0	1	0	1	n/a
Ccnd2	NM_009829	26	8	13	11	7	9	1	n/a
Lyl1	NM_008535	4573	4323	3953	4905	4293	4179	1	1.04
Pim3	NM_145478	131	84	54	83	75	81	1	-1.13
Tnfrsf13c	NM_028075	22	24	26	33	24	16	1	n/a

The total reads for each library were normalized to 20 million. Columns Con1 thru Oxm3 showed the normalized reads for each gene in different libraries. Con1, Con2, and Con3 denote library 1, 2, and 3 for placebo-treated mice, respectively, whereas Oxm1, Oxm2, Oxm3 for OXM-treated mice. A Q value lower than 0.05 was considered as significant.

AvgFC denotes average fold change. When both the average OXM read and the average placebo read were below 50, the expression level of the particular gene was deemed as too low to calculate a fold change. Instead, n/a, which denotes not applicable, was filled in the AvgFC column.

Table S7: Comparison of *Spp1* expression levels between KSL and basophilic erythroblast libraries, related to Table 2

Libary	Average normalized tag count for *Spp1*
OXM-treated KSL cells	146
Placebo-treated KSL cells	1529
OXM-treated basophilic erythroblasts	1.5
Placebo-treated basophilic erythroblasts	1.2

The total reads for each individual library were normalized to 20 million first. The tag

count for *Spp1* gene shown here was the average of all six libraries in each condition. For

any particular gene, an average tag greater than 50 was considered as true signal.

Table S8: Primers used for qPCR amplification, related to Figure 3

Name	Sequence	Note
MG3157	5' GTGGCGCGGCGACTTCCAGT 3'	For *ROSA26* transgenic allele
MG3158	5' TCCGCGTGCAGCAGATGGCG 3'	
MG1711	5' GAGCTGCCTGATACGGATGCTG 3'	For *Fancc*$^{-/-}$ allele
MG1791	5' GGGCTGCTAAAGCGCATGCTC 3'	
MG3153	5' CACGGTGTGGTGGGCCCAGGT 3'	For *Fancd2*$^{-/-}$ allele
MG3154	5' GGGAGCCCTTGCATGACAATTCTGCT 3'	
MG1711	5' GAGCTGCCTGATACGGATGCTG 3'	For *Fancc*$^{+/+}$ allele
MG1712	5' GAGAAATGGCTCAGTGGTTAAGAG 3'	
OatF	5' GCTGCCCTCTGACGTTGTGAC 3'	For *Oat* RT-PCR
OatR	5' TCGAAGTCGCAGGCACACCT 3'	
TfrcF	5' GGCGCTTCCTAGTACTCCCTTGT 3'	For *Tfrc* RT-PCR
TfrcR	5' TGCCGAGCAAGGCTAAACCG 3'	
OpnF	5' CCTCCCTCCCGGTGAAAGTG 3'	For *Spp1* RT-PCR
OpnR	5' GAGATGGGTCAGGCACCAGC 3'	
GapF	5' ATGGTGAAGGTCGGTGTGAACG 3'	For *Gapdh* RT-PCR
GapR	5' GTCAATGAAGGGGTCGTTGATGGCA 3'	